

MIT Open Access Articles

Correction of rotational distortion for catheter-based en face OCT and OCT angiography

The MIT Faculty has made this article openly available. **Please share** how this access benefits you. Your story matters.

Citation: Ahsen, Osman O., Hsiang-Chieh Lee, Michael G. Giacomelli, Zhao Wang, Kaicheng Liang, Tsung-Han Tsai, Benjamin Potsaid, Hiroshi Mashimo, and James G. Fujimoto. "Correction of Rotational Distortion for Catheter-Based En Face OCT and OCT Angiography." *Opt. Lett.* 39, no. 20 (2014): 5973.

As Published: <http://dx.doi.org/10.1364/ol.39.005973>

Publisher: Optical Society of America

Persistent URL: <http://hdl.handle.net/1721.1/100227>

Version: Author's final manuscript: final author's manuscript post peer review, without publisher's formatting or copy editing

Terms of use: Creative Commons Attribution-Noncommercial-Share Alike





Published in final edited form as:

Opt Lett. 2014 October 15; 39(20): 5973–5976.

Correction of rotational distortion for catheter-based *en face* OCT and OCT angiography

Osman O. Ahsen¹, Hsiang-Chieh Lee¹, Michael G. Giacomelli¹, Zhao Wang¹, Kaicheng Liang¹, Tsung-Han Tsai¹, Benjamin Potsaid^{1,2}, Hiroshi Mashimo^{3,4}, and James G. Fujimoto^{1,*}

¹Department of Electrical Engineering and Computer Science and Research Laboratory of Electronics, Massachusetts Institute of Technology, Cambridge, Massachusetts 02139, USA

²Advanced Imaging Group, Thorlabs Inc., Newton, New Jersey 07860, USA

³Veterans Affairs Boston Healthcare System, Boston, Massachusetts 02130, USA

⁴Harvard Medical School, Boston, Massachusetts 02115, USA

Abstract

We demonstrate a computationally efficient method for correcting the nonuniform rotational distortion (NURD) in catheter-based imaging systems to improve endoscopic *en face* optical coherence tomography (OCT) and OCT angiography. The method performs nonrigid registration using fiducial markers on the catheter to correct rotational speed variations. Algorithm performance is investigated with an ultrahigh-speed endoscopic OCT system and micromotor catheter. Scan nonuniformity is quantitatively characterized, and artifacts from rotational speed variations are significantly reduced. Furthermore, we present endoscopic *en face* OCT and OCT angiography images of human gastrointestinal tract *in vivo* to demonstrate the image quality improvement using the correction algorithm.

Nonuniform rotational distortion (NURD) is a common problem in catheter-based imaging systems such as intravascular and endoscopic optical coherence tomography (OCT) and ultrasound [1, 2]. Conventional catheter-based imaging systems employ proximal actuation to rotate the optical assembly and generate a circumferential scan. In these systems, NURD is observed for both *in vivo* human and *ex vivo* phantom studies, suggesting that it is inherently present due to mechanical friction between the catheter torque coil and sheath [1, 2]. Physiological motion as well as bends encountered in endoscopic and cardiovascular imaging applications can exacerbate the severity of the rotational nonuniformity.

Micromotor catheters perform distal rotational scanning and eliminate some of the aforementioned problems associated with proximal rotation [3, 4]. Rotation speed as high as 3.2 kHz was reported with a micromotor catheter, which cannot be attained by proximal actuation [5]. Unfortunately, NURD is still observed in micromotor imaging catheters due to motor mechanical instability, although it is significantly less than in proximally actuated

catheters [6]. A motor with an encoder or other closed-loop feedback would improve the uniformity of the rotation, but the increased size might not be suitable for clinical applications.

Several methods have been demonstrated to correct NURD in catheter-based imaging systems, such as registering neighboring A-lines or frames by maximizing cross-correlation signal intensity [2,7–9], or using structural landmarks (e.g., stent struts) to aid registration of subsequently acquired datasets [10]. The reflections from the sheath or optical components of the catheters are also used for correcting rotational fluctuations caused by NURD [11]. However, methods using cross-correlation or phase information typically require highly correlated images. Some methods require disabling the longitudinal scan (pullback) entirely [7, 11], or provide only moderate improvement in rotational uniformity when tested *in vivo* [2, 7]. For catheter-based applications with significant patient or operator motion, methods that do not rely on dynamic image features for correction may be desirable.

With recent advances in OCT speed, rapid volumetric imaging became possible. Following these developments, *en face* OCT is emerging as a powerful tool, especially for assessing ocular pathology [12]. Furthermore, OCT angiography was developed as a functional extension of OCT, enabling three dimensional visualization of vasculature without requiring exogenous contrast agents [13, 14]. OCT angiography using OCT signal intensity has several advantages over phase-sensitive techniques such as Doppler OCT or phase-variance OCT, including relaxed system phase stability requirements and good sensitivity to slow blood flow occurring in capillaries [15, 16]. Our group recently demonstrated the combination of high-speed imaging and distal rotation to achieve highly stable scanning required for assessment of *en face* mucosal patterns and for endoscopic OCT angiography [17]. However, visualizing fine details with *en face* OCT or performing endoscopic OCT angiography further increases scanning uniformity requirements.

In this Letter, we present a computationally efficient method for correcting the NURD encountered in catheter- based OCT. The method uses fiducial markers located on the catheter and resamples the cross-sectional images in accordance with the detected marker positions. We characterize the magnitude and frequency spectra of the rotational nonuniformity, and quantify NURD correction algorithm accuracy. We also present exemplary *en face* OCT and OCT angiograms acquired with an ultrahigh-speed endoscopic OCT system *in vivo* to show the image quality improvement.

This study was conducted using an ultrahigh-speed endoscopic-swept source OCT system with a VCSEL and micromotor catheter, as described in reference [18]. Briefly, the VCSEL operated at 300 kHz bi-directional sweep rate and 120-nm tuning range, enabling 600-kHz A-line rate and 8- μm axial resolution in tissue, respectively. The A/D card (ATS9360, AlazarTech) was optically clocked at 1.1 GHz maximum clock frequency, resulting in a 3.3-mm imaging range in air. We used a micromotor catheter with a 3.2-mm outer diameter (OD), which passed through the 3.7-mm endoscope accessory port. The distal part of the catheter consisted of a ferrule, GRIN lens, and prism mounted on the micromotor shaft. The spot size was $\sim 15\ \mu\text{m}$ (FWHM) in tissue. The micromotor rotated at 400 Hz, and the catheter was proximally pulled back at 2 mm/s. Each dataset consisted of 3200 frames with

1500 A-lines per frame. This resulted in a sampling pitch of $6.7\ \mu\text{m}$ in rotation and $5\ \mu\text{m}$ in pullback.

NURD correction was performed on sequential cross-sectional rotary OCT images in linear intensity scale prior to generating *en face* OCT images and OCT angiograms. *En face* OCT image stacks were then generated from the NURD-corrected 3D-OCT datasets with square root compression and projected over $140\ \mu\text{m}$ depth at various depth levels. Endoscopic OCT angiography was performed by calculating the intensity decorrelation between sequential frames, similar to reference [19]. This requires spatially overlapping cross-sectional images in the pullback; hence images are intentionally oversampled in this direction. Following decorrelation calculation, three consecutive decorrelation images are averaged to reduce noise, and intensity thresholded to remove noise from low signal regions. Finally, *en face* OCT angiograms were generated from the cross-sectional OCT angiography stacks and projected over a $140\ \mu\text{m}$ range at various depth levels.

Imaging was performed on patients at the Boston VA Healthcare System (VABHS) under IRB-approved protocols, and written informed consent was obtained prior to the study.

Figure 1 shows an example OCT image and a drawing of the catheter imaging probe. Figure 1(a) is an *in vivo* image of the human esophagus which corresponds to a single rotary scan of the catheter micromotor. The OCT image shows four fiducial positions that are created by the micromotor mount in Fig. 1(b). The fiducials could also be placed on the catheter sheath.

The NURD correction algorithm operates by detecting the fiducial positions on sequential OCT images, corresponding to sequential rotary scans. The fiducials correspond to fixed angular positions or fixed circumferential positions in the scan, but NURD causes the fiducial to appear at varying times or A-line positions. It is important to note that NURD causes not only a timing jitter (translation) in the positions of sequential OCT images, but also stretching or compression of images in the transverse direction, because the rotational period and the number of A-lines per rotation are varying.

The volumetric OCT dataset is composed of sequential cross-sectional OCT images from rotary scans sampled at constant A-scan rate. The OCT data is generated with a constant transverse-pixel sampling rate, but varying angular/circumferential velocity. The objective of the NURD correction algorithm is to resample the volumetric OCT data such that the transverse pixels correspond to registered and equally spaced angular/circumferential positions, correcting for both timing jitter (translation) and stretching/compression of the OCT images in successive rotary scans. This resampling process is somewhat analogous to resampling the OCT spectrum from lambda to constant frequency or k interval, which occurs in spectral domain OCT. The positions of the fiducials are used to generate a cubic spline resampling, which is continuous in position as well as first and second derivative of the position in time, corresponding to the assumption that the rotation has continuous velocity and acceleration.

Using more than one fiducial per rotation will increase the number of angular/circumferential reference locations and improve the accuracy of the resampling. This resampling essentially performs a nonrigid registration in the transverse direction. The axial

position of the image is assumed to be constant because tissue is in contact with the catheter sheath.

Two fiducials per rotation were used to measure the NURD. As shown in Fig. 2(a), without NURD correction, the angular deviation of the fiducial in sequential frames oscillates significantly with a standard deviation of 16.4 mrad (26.2 μm in circumferential position assuming 3.3-mm probe OD). The mean value of the angular deviation for 10 different acquisitions on different patients was 16.8 mrad (min = 10 mrad, max = 26 mrad, coefficient of variation = 0.3). The frequency analysis in Fig. 2(c) shows this variation has a significant component around 130 Hz. This instability appears to be from the micromotor and was observed in multiple different catheters. Additional measurements by placing multiple photodetectors around the probe (*ex vivo*) were performed to confirm that this was not aliased from higher frequencies. Following the Nyquist criteria, using two fiducials per rotation for NURD correction, i.e., sampling at twice the rotation frequency, can correct instabilities up to 400 Hz for the parameters in this study.

To quantify the correction algorithm performance, we used two fiducials per rotation for stabilization [e.g., A and C shown in Fig. 1(a)], and two other fiducials for measurement [e.g., B and D shown in Fig. 1(a)]. Measurements show the angular deviation is significantly reduced. Following NURD correction, the angle standard deviation is reduced to 1 mrad (1.7 μm in circumference assuming 3.3-mm probe OD), equivalent to a greater than 15-fold improvement in rotational stability [Fig. 2(b)]. Figure 2(d) further illustrates the improvement in rotational stability at 130 Hz as well as at other frequency components. The mean value of the angular deviation for 10 different acquisitions on different patients was 1.4 mrad (min = 0.9 mrad, max = 1.7 mrad, coefficient of variation = 0.2).

Figure 3 shows the performance of the correction algorithm for endoscopic OCT images of the human GI tract. Figures 3(a) and 3(c) show *en face* OCT images acquired from the rectum of a patient before and after NURD correction, where regular crypt architecture (pit pattern) can be observed, characteristic of normal colon. Without NURD correction, severe distortion can be observed in the *en face* pit patterns, as shown in Fig. 3(a). Figure 3(c) shows the distortions are significantly reduced with NURD correction. Figures 3(b) and 3(d) show endoscopic OCT angiograms from the esophagus of a patient. Before correction, OCT angiography images exhibit decorrelation artifacts due to rotational instability between consecutive frames. This results in increased OCT angiography background noise and vertical streaks along the pullback direction [Fig. 3(b)]. As shown in Fig. 3(d), the algorithm improves registration of consecutive frames, reducing decorrelation noise and improving angiography quality.

The scanning parameters in these experiments yielded sampling pitches of 6.7 and 5 μm along the rotation and pullback direction, respectively. Given the 15 μm spot size, even very small scanning instabilities will cause significant decorrelation noise between adjacent frames. Furthermore, because a helical pullback scanning is typically used for catheter-based imaging systems, it is not possible to acquire several repeated frames at precisely the same longitudinal location, in contrast to ophthalmic OCT angiography, which uses galvanometer scanning. NURD correction addresses rotational instability, but endoscopic OCT

angiography is still limited by pullback instability. Pullback instability might be corrected by using fiducials on the catheter sheath.

In addition, other instabilities arise from the relative movement of the tissue with respect to the catheter. This causes large-scale image distortion in the 3D-OCT data and uncertainty in registration relative to the tissue. Using fiducial markers that are located on the catheter will not correct for tissue motion. However, this study was less vulnerable to tissue motion, due to the ultrahigh speed acquisition.

The applicability of the fiducial marker method requires minimal modification of catheter design. For micromotor catheters, the housing struts or shadows from cables can be used as inherent fiducials. Rotational as well as longitudinal fiducial lines can be printed or laser etched on the inner or outer surfaces or even internal to the transparent probe sheath. The number of fiducial markers required to effectively suppress the NURD will depend on the rotation stability and the frequency of the dominant instabilities.

In conclusion, a computationally efficient method is demonstrated that corrects image distortion from rotational nonuniformity. This method can be used to effectively correct instabilities up to a Nyquist frequency determined by the temporal spacing between two serially detected fiducial markers. By increasing the number of fiducials, the correction accuracy can be improved. Our study shows that two fiducial markers per frame are sufficient to effectively suppress the NURD in high-speed micromotor endoscopy and provide a nondistorted *en face* or angiographic image. However larger diameter-imaging probes would require larger numbers of fiducials. This method can be applied to both proximally and distally actuated catheter designs. Due to its accuracy and suitability for high-speed imaging, this correction method could be a valuable tool for next-generation endoscopic and cardiovascular OCT systems that acquire combined structural and functional image information to assess pathological and physiological markers of disease.

Acknowledgments

We would like to thank to Marisa Figueiredo and Qin Huang at VABHS for clinical assistance in patient recruitment and pathology reading, Martin Kraus at MIT/Erlangen for helpful discussions and software assistance, as well as Thorlabs, Inc. for providing the VCSEL module used in this study. Tsung-Han Tsai's current address is St. Jude Medical, Inc. This work was supported in part by the National Institutes of Health R01-EY011289-26, R44-EY022864-01, R01-CA075289-16, R44-CA101067-05, R01-CA178636-02 and Air Force Office of Scientific Research AFOSR contracts FA9550-10-1-0063 and FA9550-12-1-0499.

References

1. Kawase Y, Suzuki Y, Ikeno F, Yoneyama R, Hoshino K, Ly HQ, Lau GT, Hayase M, Yeung AC, Hajjar RJ. *Ultrasound Med. Biol.* 2007; 33:67. [PubMed: 17189048]
2. Kang W, Wang H, Wang Z, Jenkins MW, Isenberg GA, Chak A, Rollins AM. *Opt. Express.* 2011; 19:20722. [PubMed: 21997082]
3. Herz PR, Chen Y, Aguirre AD, Schneider K, Hsiung P, Fujimoto JG, Madden K, Schmitt J, Goodnow J, Petersen C. *Opt. Lett.* 2004; 29:2261. [PubMed: 15524374]
4. Tran PH, Mukai DS, Brenner M, Chen Z. *Opt. Lett.* 2004; 29:1236. [PubMed: 15209258]
5. Wang T, Wieser W, Springeling G, Beurskens R, Lancee CT, Pfeiffer T, van der Steen AF, Huber R, van Soest G. *Opt. Lett.* 2013; 38:1715. [PubMed: 23938921]

6. Li JA, de Groot M, Helderma F, Mo JH, Daniels JMA, Grunberg K, Sutedja TG, de Boer JF. *Opt. Express*. 2012; 20:24132. [PubMed: 23187176]
7. van Soest G, Bosch JG, van der Steen AF. *IEEE Trans. Inf. Technol. Biomed.* 2008; 12:348. [PubMed: 18693502]
8. Gatta C, Pujol O, Leor OR, Ferre JM, Radeva P. *IEEE Trans. Info. Technol. B.* 2009; 13:1006.
9. Yin J, Liu G, Zhang J, Yu L, Mahon S, Mukai D, Brenner M, Chen Z. *J. Biomed. Opt.* 2009; 14:060503. [PubMed: 20059234]
10. Ughi GJ, Adriaenssens T, Larsson M, Dubois C, Sinnaeve PR, Coosemans M, Desmet W, D'Hooge J. *J. Biomed. Opt.* 2012; 17:026005. [PubMed: 22463037]
11. Sun C, Nolte F, Cheng KH, Vuong B, Lee KK, Standish BA, Courtney B, Marotta TR, Mariampillai A, Yang VX. *Biomed. Opt. Express*. 2012; 3:2600. [PubMed: 23082299]
12. Lumbroso B, Huang D, Romano A, Rispoli M, Coscas G. *Clinical En Face OCT Atlas (JP Medical Ltd.* 2013
13. Wang RK, Jacques SL, Ma Z, Hurst S, Hanson SR, Gruber A. *Opt. Express*. 2007; 15:4083. [PubMed: 19532651]
14. Yasuno Y, Hong YJ, Makita S, Yamanari M, Akiba M, Miura M, Yatagai T. *Opt. Express*. 2007; 15:6121. [PubMed: 19546917]
15. Mariampillai A, Standish BA, Moriyama EH, Khurana M, Munce NR, Leung MKK, Jiang J, Cable A, Wilson BC, Vitkin IA, Yang VXD. *Opt. Lett.* 2008; 33:1530. [PubMed: 18594688]
16. Tokayer J, Jia Y, Dhalla AH, Huang D. *Biomed. Opt. Express*. 2013; 4:1909. [PubMed: 24156053]
17. Tsai T-H, Ahsen OO, Lee H-C, Liang K, Figueiredo M, Tao YK, Giacomelli MG, Potsaid BM, Jayaraman V, Huang Q, Cable AE, Fujimoto JG, Mashimo H. Endoscopic optical coherence angiography enables three dimensional visualization of subsurface microvasculature. *Gastroenterology*.
18. Tsai T-H, Ahsen OO, Lee H-C, Liang K, Giacomelli MG, Potsaid BM, Tao YK, Jayaraman V, Kraus MF, Hornegger J, Figueiredo M, Huang Q, Mashimo H, Cable AE, Fujimoto JG. *Proc. SPIE*. 2014; 8927:89270T.
19. Jonathan E, Enfield J, Leahy MJ. *J. Biophotonics*. 2011; 4:583. [PubMed: 21887769]

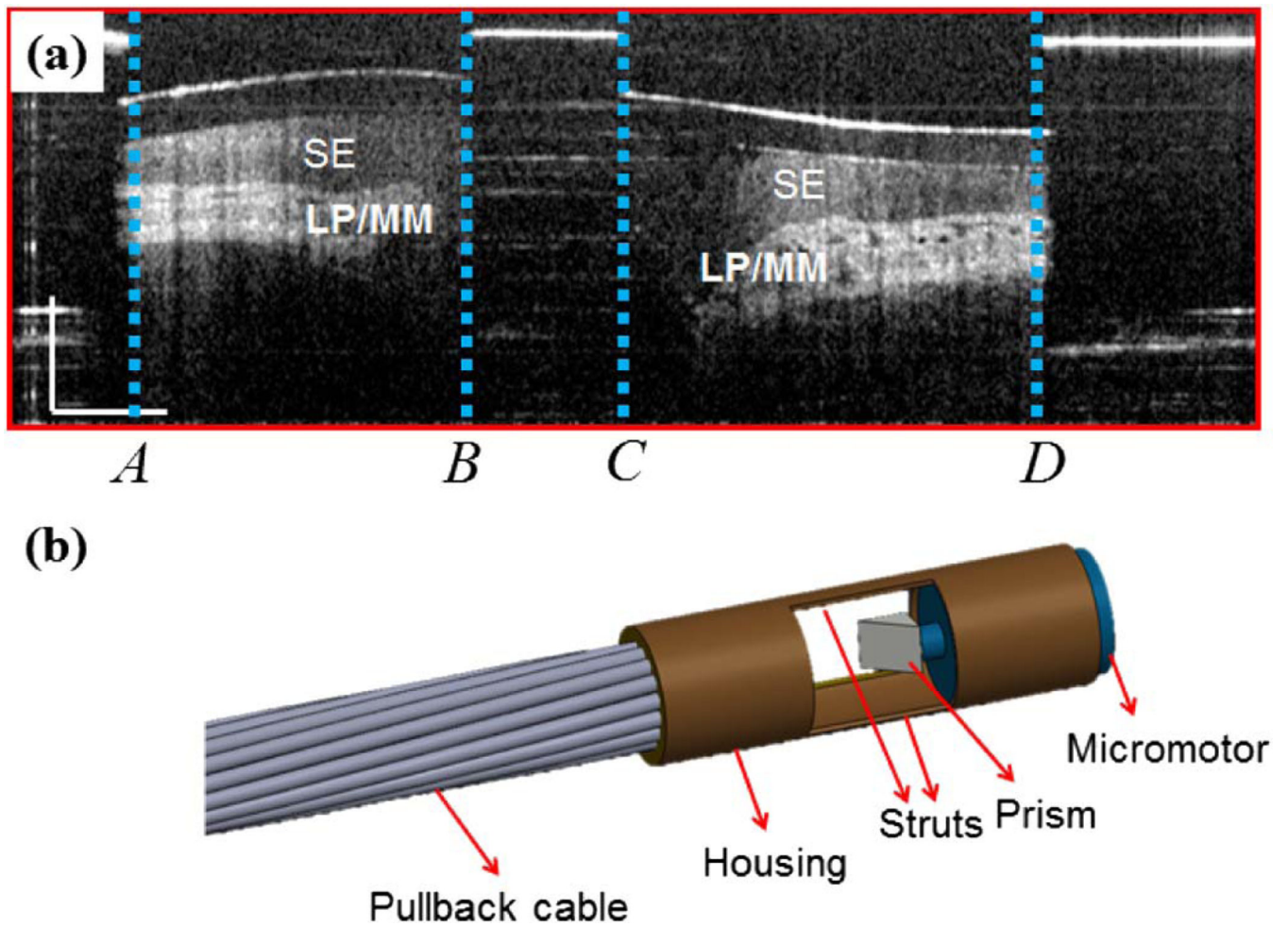


Fig. 1. Description of the fiducial marker NURD correction algorithm for a micromotor catheter. (a) Example OCT image showing fiducial positions. (b) Drawing of a micromotor catheter with two struts and two imaging windows generating four fiducial positions. SE: Squamous epithelium, LP/MM: Lamina propria/Muscularis mucosa. Scale bars are 1 mm.

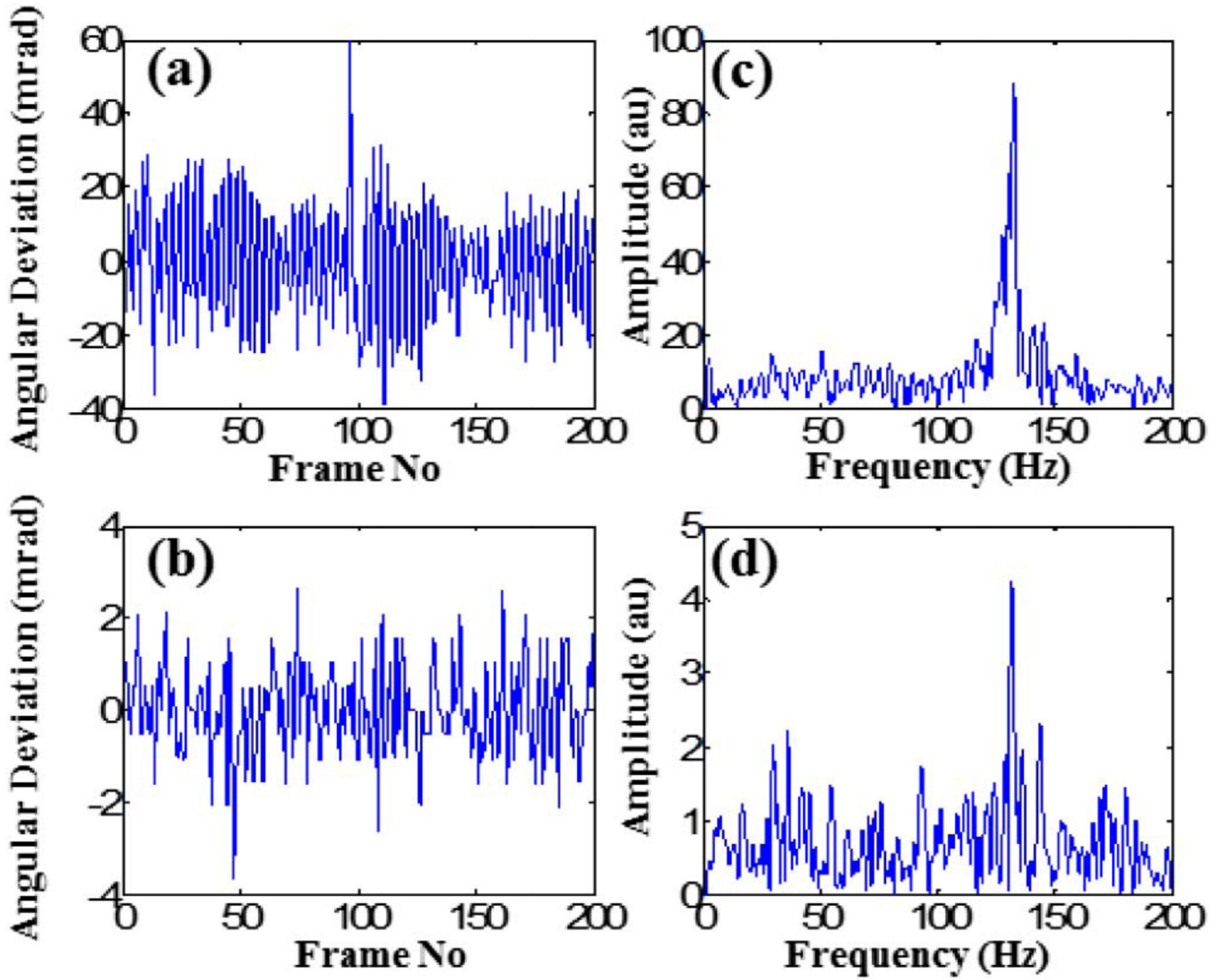


Fig. 2. Characterization of NURD before and after software correction. (a) Temporal positions of a fiducial from 200 sequential frames prior to correction (around zero mean). (b) Temporal position of a fiducial (not used for correction) from 200 sequential frames postcorrection (around zero mean). (c), (d) Fourier transforms of the waveforms from (a) and (b), respectively.

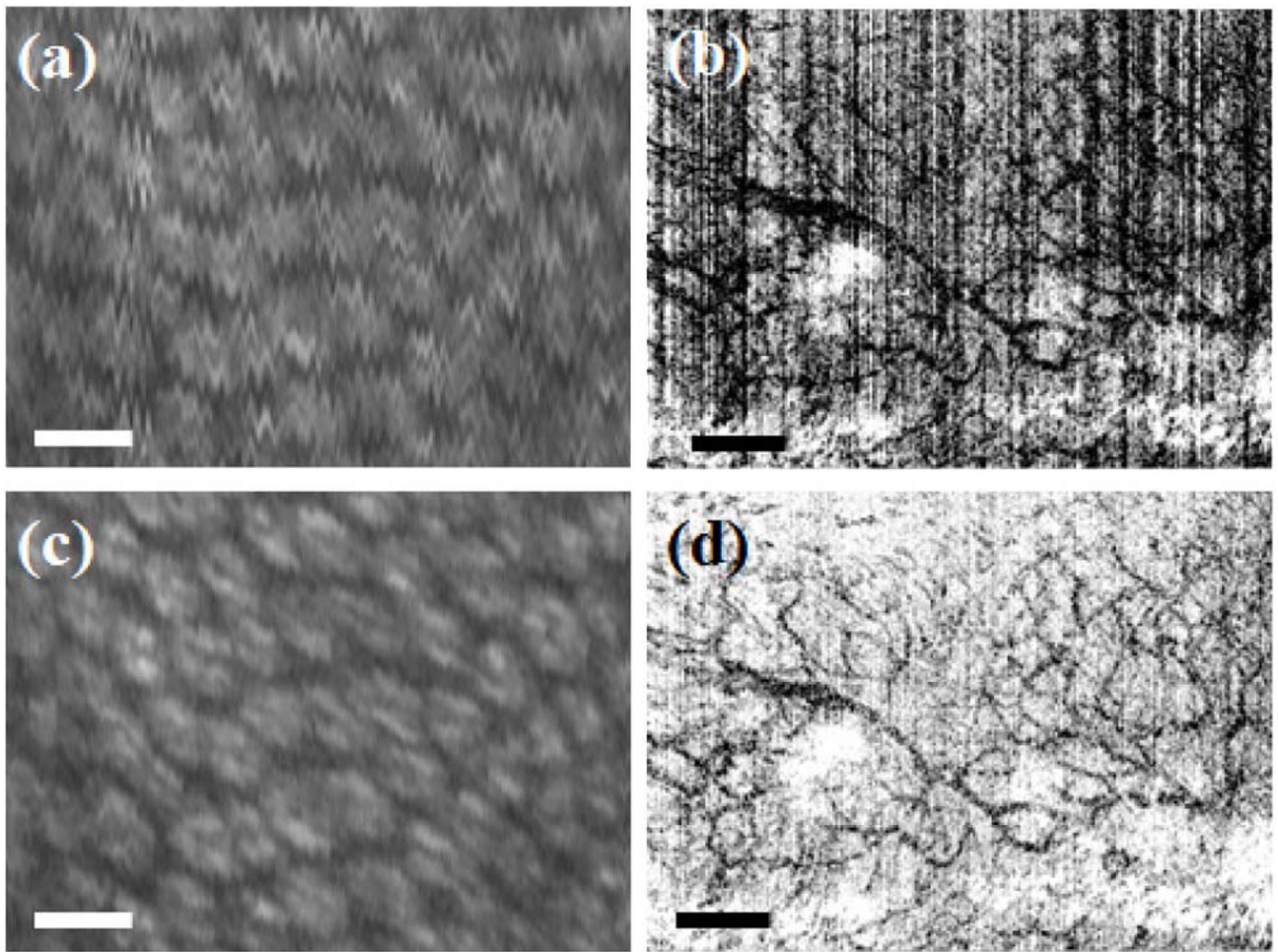


Fig. 3. Demonstration of the NURD correction algorithm for *en face* OCT and OCT angiography images. (a) and (c) show *en face* OCT images before and after applying the correction algorithm, respectively. (b) and (d) show OCT angiograms before and after applying the correction algorithm, respectively. All figures are generated by projection over 140 μm of depth, and about 150–500 μm beneath tissue surface. (a) and (c) are taken from the rectum, and (b) and (d) are taken from esophagus of two patients who were undergoing endoscopic surveillance. Same signal thresholds are applied for (a) and (c), and for (b) and (d). Scale bars are 200 μm for (a) and (c), and 500 μm for (b) and (d).